Refinement of the Crystal Structure of Ribonuclease S. Comparison with and between the Various Ribonuclease A Structures[†,‡]

Eunice E. Kim, Raghavan Varadarajan,[§] Harold W. Wyckoff, and Frederic M. Richards[*]

Department of Molecular Biophysics and Biochemistry, Yale University, New Haven, Connecticut 06511

Received December 20, 1991; Revised Manuscript Received May 27, 1992

ABSTRACT: Ribonuclease S (RNase-S) is a complex that consists of two proteolytic fragments of bovine pancreatic ribonuclease A (RNase-A): the S-peptide (residues 1–20) and S-protein (residues 21–124). We have refined the crystal structures of three RNase-S complexes. The first two contain the full-length 20-residue S-peptide and were studied at pHs of 4.75 and 5.5. The third one consists of a truncated form of S-peptide (residues 1–15) and was studied at pH 4.75 as the reference structure for a series of mutant peptide complexes to be reported separately. Excluding residues 16–23 which are either missing (in the S15 complex) or disordered (in both S20 complexes), all three structures refined at 1.6-Å resolution are identical within the estimated errors in the coordinates (0.048 Å for the backbone atoms). The *R*-values, residual error, range from 17.4% to 18.6%. The final model of S20, pH 4.75, includes 1 sulfate and 84 water molecules. The side chains of 11 residues were modeled in two discrete conformations. The final structures were independent of the particular RNase-A or RNase-S used as a starting model. An extensive comparison with refined crystal structures of RNase-A reveals that the core of the molecule which is held together with extensive hydrogen bonds is in identical pattern in all cases. However, the loop regions vary from one structure to another and are often characterized by high *B*-factors. The pattern of thermal parameters appears to be dependent on crystal packing and correlates well with the accessibility calculated in the crystal. Gln60 is a conserved residue in all sequences known to date for this class of ribonucleases. However, it is the only residue that is clearly defined in an unfavorable position ($\phi = -100°$, $\psi = -130°$) on the Ramachandran plot. The origin of the substantial differences between RNase-A and RNase-S in stability to both acid and temperature denaturation and in susceptibility to proteolysis at neutral pH is not obvious in our visual comparison of these two structures.

Bovine pancreatic ribonuclease (RNase-A) is one of the best characterized ribonucleases [for reviews see Richards and Wyckoff (1971) and Blackburn and Moore (1982)]. It consists of a single chain of 124 amino acids (M_r = 13 683). When subjected to limited digestion by subtilisin, the peptide bond between residues Ala20 and Ser21 is cleaved (Richards & Vithyathil, 1959). The two fragments, S-peptide (residues 1–20) and S-protein (residues 21–124), can be separated and reconstituted to give the fully active complex ribonuclease S (RNase-S).

The crystal structures of RNase-A and RNase-S were determined independently (Kartha et al., 1967; Wyckoff et al., 1967a,b), and the two proteins have very similar structures. However, there are significant differences in the stabilities of the two proteins to acid (Takahashi et al., 1969) and temperature-induced denaturation (Sherwood & Potts, 1965), as well as susceptibility to further proteolysis (Allende & Richards, 1962). Residues 3–13 of the peptide portion of RNase-S form an α-helix, just as they do in the uncleaved RNase-A. Residues 16–20 are not clearly defined in the crystal structure of RNase-S (Wyckoff et al., 1970), and these residues are not important for binding, since a complex of a peptide containing only the first 15 residues of S-peptide with S-protein has been shown to be structurally identical to that of RNase-S with a 20-residue peptide (Taylor et al., 1981). We have refined, and reported here, the crystal structures of RNase-S, with the conventional S-peptide of 20 residues (S20) at two different pHs (4.75 and 5.5) and with a truncated S-peptide consisting of only the first 15 residues (S15) at pH 4.75. Two pHs were chosen: pH 5.5, because most of the previous studies were done at this pH where K_m is minimal, and pH 4.75, to ensure more complete SO_4 binding in the crystal.

The second part of this paper consists of detailed comparisons of the refined structures of RNase-S and RNase-A. Earlier, it was noted that there are structural differences between RNase-A and RNase-S (Wlodawer et al., 1982). However, this was based on a comparison of a refined model of RNase-A and an unrefined model of RNase-S, both at 2.0-Å resolution. Since then the crystal structure of RNase-A has been refined by several independent investigators at high resolution (see Table VI for references). The crystals used in these studies were grown using different conditions of solvent and pH. Also, the studies employed different methods of data collection and used different refinement algorithms. It is of interest to compare these structures with each other as well as with RNase-S in order to examine the range of conformations accessible to the enzyme in the crystals. Rico et al. (1989) also reported differences in the two enzymes in solution structures determined by NMR.

MATERIALS AND METHODS

(*a*) *Purification and Crystallization.* Bovine pancreatic RNase-S was obtained from Sigma Chemical Co. in the form of a lyophilized powder. For crystallization of the S20 complex

[†] We acknowledge the support of the National Institute of General Medical Sciences (Grant GM-22778) and partial support from Miles Inc. R.V. was supported by a postdoctoral fellowship from the Damon Runyon–Walter Winchell Cancer Fund.

[‡] The atomic coordinates for the three structures reported here have been deposited in the Protein Data Bank. The PDB file names are 2RNS (S20, pH 4.75), 1RNU (S20, pH 5.5), and 1RNV (S15, pH 4.75).

[*] Author to whom correspondence should be addressed.

[§] Present address: Molecular Biophysics Unit, Indian Institute of Science, Bangalore 560 012, India.

0006-2960/92/0431-12304$03.00/0

this protein was dissolved in a solution of 6.0 M CsCl and 0.1 M sodium acetate buffer (pH 4.75 or pH 5.5) at room temperature. To this was added an equal volume of 80% saturated $(NH_4)_2SO_4$ and 0.1 M sodium acetate buffer at the selected pH. The final protein concentration was 12.5 mg/mL in each case. A drop was transferred to a glass slide with a depression, and the slide was sealed with a cover slip. Usable crystals of Y-form (Wyckoff et al., 1970; space group $P3_121$, $a = b = 44.65$ Å, $c = 97.15$ Å) were obtained after a few days at room temperature.

In the case of the S15 complex, the S-protein was prepared from RNase-S by the method of Doscher and Hirs (1967) and stored either lyophilized or as a frozen solution at −20 °C. The S-protein concentration was determined using an extinction coefficient of 9.56 mM^{-1} cm^{-1} (Connelly et al., 1990). The truncated S-peptide of S15 was synthesized as a C-terminal amide by Multiple Peptide Systems Inc., San Diego, CA. Crude peptide was purified by reverse-phase HPLC using a Vydac C-18 preparative column. The purity of the peptide was checked by fast atom bombardment mass spectrometry as reported (Connelly et al., 1990), and the peptide was stored either lyophilized or as a frozen solution at −20 °C. Peptide stock solutions were quantitated using amino acid analysis. S-Protein and S-peptide (1–15) in water were mixed together in a molar ratio of 1:3. The final S-protein concentration was approximately 1 mg/mL. The complex was lyophilized and immediately redissolved in 6.0 M CsCl and 0.1 M acetate buffer at pH 4.75. To this was added an equal volume of 70% saturated $(NH_4)_2SO_4$ and 0.1 M acetate buffer at pH 4.75. The final protein concentration was about 4–6 mg/mL. As with the S20 complex, usable crystals were obtained after a few days at room temperature.

(*b*) *Data Collection.* The crystals were stabilized in 75% saturated $(NH_4)_2SO_4$ at the desired pH, and CsCl was washed out by repeated buffer changes as described earlier (Wyckoff et al., 1970). The size of crystals used for data collection were of the order of 0.6 × 0.6 × 0.4 mm^3. Crystals were mounted in 1.0-mm glass capillaries with a small amount of mother liquor on one side. All of the data sets used in this study were collected on the San Diego Multiwire System area detectors at Yale University. The Cu Kα radiation from a Rigaku RU300 rotating anode generator operating at 50 kV and 200 mA and equipped with a graphite monochromator and a collimator with 0.5-mm diameter was used. Each frame was a 20-s exposure with 0.1° sweep.

S20 and S15 both crystallized in the same space group with similar unit cell parameters as shown in Table I. These values are comparable to the parameters of the Y-form previously described (Wyckoff et al., 1970). The dependence of the cell parameters on pH was also noted earlier (Wyckoff et al., 1970).

Each data set was collected on a single crystal at room temperature, and the data were reduced and averaged using the software provided (Howard et al., 1985). Radiation damage in each case was monitored by measuring a 5° wedge of data periodically during the data collection. It did not exceed 10%. Further scaling and rejection of weak reflections were carried out using the PROTEIN package (Steigemann, 1982). Table I summarizes some of the results from the data collection.

(*c*) *Refinement and Structure Comparison.* The starting model used for this study is from the earlier refinement of RNase-S at 2.0-Å resolution using a difference Fourier algorithm (RNASE7B, which is refined model of 1RNS, $R = 0.31$; Powers, 1976). Refinement was carried out mostly

Table I: Summary of Data and Refinement of RNase-S Crystals[a]

S-peptide	1–20	1–20	1–15
S-protein	21–124	21–124	21–124
pH	5.50	4.75	4.75
PDB file name	1RNU	2RNS	1RNV
$a = b$ (Å)	44.68	44.50	44.45
c (Å)	97.03	97.62	97.60
total no. of obs	76450	81490	93541
no. of unique refl	15104	14870	14562
possible no. for 1.6 Å	15437	15398	15364
av $I/\sigma(I)$	12.2	10.3	13.1
R_{merge} (%)	5.4	5.8	5.7
resolution (Å)	8.0–1.6	8.0–1.6	8.0–1.6
no. of refl refined	14924	14667	14163
R_{final} (%)	17.6	17.4	18.6
R_{-water}	22.7	22.4	23.5
no of waters	88	84	70
no. of residues in two conf	11	11	8
rms deviations in			
bond lengths (Å)	0.012	0.013	0.013
bond angles (deg)	2.75	2.84	2.79
av B-factor (Å^2)[b]			
main chain	21.0	20.7	21.2
side chain	34.1	33.9	35.4

[a] The space group for all crystals was $P3_121$. Earlier cell parameters from Wyckoff et al. (1970) with crystals equivalent to the complex S20: $a = b = 44.65$ Å, $c = 97.15$ Å (pH 5.5); $a = b = 44.38$ Å, $c = 97.94$ Å (pH 4.9). [b] These values are excluding residues 16–23.

using X-PLOR (Brünger, 1990), but an FFT-implemented version (PROFFT; Finzel, 1987) of the stereochemically restrained least-squares refinement method (Hendrickson, 1985) was used during the beginning stages of this study. Refinement was carried out using simulated annealing with the slow cooling protocol of X-PLOR (Brünger et al., 1990). The calculations were done on the VAX 8800 and CONVEX C-2 at the Center for Structural Biology at Yale. Manual model building was done against $2F_o - F_c$ and $F_c - F_c$ difference Fourier maps as well as omit maps using FRODO (Jones, 1982) on an Evans and Sutherland PS390 graphics system. Omit maps were generated after simulated annealing of a model in which atoms that are within a certain radius from the atom in question were omitted (always less than 10% of the total) in structure factor calculations in order to avoid model bias.

Waters were picked on the basis of the peak heights and distance criteria (2.4–3.6 Å) from the difference map, but they were inspected against both the $2F_o - F_c$ and the difference maps. All waters were assigned unit occupancy. Those waters whose temperature factors were above 80.0 after refinement with no restraints on the B-factor, or were not above 0.8σ in the $2F_o - F_c$ map, were removed from the list.

In order to estimate errors in the coordinates due to lack of convergence or trapping in false minima, six different X-PLOR protocols were run for the S15 complex. Each protocol used a different starting temperature and/or time step during the dynamics simulations (details of the protocols used and the results are available as supplementary material). The model was refined against S15 data using the reflections between 8.0 and 1.65 Å that have $F_o \geq 4\sigma$. In each case the individual temperature factors were refined without restraints, starting from the same values.

Difference distance matrices (Kundrot & Richards, 1987a) were used to examine differences between the structures. Solvent-accessible surface areas were calculated using ACCESS (Richards, 1985) following the method of Lee and Richards (1971). A probe sphere with radius of 1.4 Å was used. The program INSIGHT (Biosym Technologies, San

Diego, CA) was also used for superpositioning of the various structures.

Some refinements for the S15 complex were also carried out using the previously refined RNase-A structures (see Table VI) as starting models. These were refined against S15 data, using reflections between 8.0 and 1.65 Å that have $F_o \geq 4\sigma$. The starting RNase-A models used included (1) a hybrid model, region 62–73 of the RNase-S molecule replaced by that of the RNase-A model (PAUL; Harkins, private communication, 1991), (2) 7RSA (Wlodawer et al., 1988) omitting residues 16–23, and (3) PAUL (Harkins) omitting residues 16–23. All these were obtained by superposing the corresponding RNase-A structure onto the refined RNase-S structure using only the backbone (N, C, O, and Cα) and Cβ atoms of residues between 24 and 123 by a least-squares method. All refinements were carried out using simulated annealing. The rms differences ranged from 0.59 to 0.74 Å.

RESULTS AND DISCUSSION

(1) Refinement of RNase-S. (a) Overall Structure and Summary of Refinement. The final model of RNase-S (S20) includes 952 protein non-hydrogen atoms (923 in the case of S15), 1 sulfate, and 84 water molecules. The results of the final refinement using all data from 8.0 to 1.60 Å are summarized in Table I. The side chains of 11 residues were modeled in two discrete conformations. In the final model all of the included waters were refined with an occupancy of 1.0. The resulting three structures are almost identical [see Richards and Wyckoff (1971) for detailed description of the structure], i.e., within the estimated coordinate error described in section g, except at positions 1–3 and 16–23. Table II lists H-bonds and changes in the accessible surface areas due to interactions between the S-peptide and S-protein. The Cα trace is shown in Figure 1 together with that of selected RNase-As. Unless mentioned specifically, the following general description applies to all three structures.

Except for residues 16–23 most of the structure is clearly defined in the $2F_o - F_c$ maps. There is no appreciable electron density for these eight residues in any of the maps. When residues 16–23 are excluded from the refinement, the overall *R*-value increases by 0.2–0.3%, and the maps are almost identical. For the two S20 structures there are no breaks in the electron density maps for the backbone atoms when contoured at a 1.5σ level (σ is the rms deviation of electron density from the average, not an error estimate in the map), but several of the side-chain atoms are not well defined. For S15, however, there are breaks at the backbone atoms of residues 89–90 and 112–114, residues 66–70 are poorly defined in the electron density maps, and a larger number of side-chain atoms have truncated density. Overall, the electron density map of S15 is visibly noisier than those of S20. Also, the *R*-value is higher as shown in Table I. This observation was surprising and not expected. The reason for the difference is not clear.

Although not used in the final models reported in Table I, we tried refinement using weights of $1/\sigma^2$ for each reflection, the σ being the σ values from data reduction (Howard et al., 1985). However, this weighting scheme resulted in an increase in the *R*-value by about 2.0%. When the reflections with only $F_o \geq 2\sigma$ (98% of the total number of reflections in the case of S20, pH 4.75) were used for the unweighted refinement, the overall *R*-value was not affected measurably. However, the overall *R*-value improved when only the reflections with $F_o \geq 4\sigma$ were included in the refinement. For example, in the case of S15 it is improved by about 1.5%, but this meant that 12% of the total reflections were excluded. The final *R*-values are slightly higher than the values found in some other structures at comparable resolution (Katti et al., 1990; Blevins & Tulinski, 1985). We note that approximately 5% of the structure is disordered and the average temperature factors for all three structures are higher than those reported for RNase-A (see Figure 7), indicating a greater degree of disorder in RNase-S.

Table II: Interactions between S-Peptide and S-Protein

S-peptide	Hydrogen Bonds S-protein	distance (Å)
10 Arg O	33 Arg NH_2	2.81
10 Arg NH2	33 Arg O	2.79
11 Gln O	44 Asn ND2	2.81
12 His O	47 Val N	2.73
12 His ND1	45 Thr O	2.80
13 Met O	33 Arg NH1	2.97
13 Met O	33 Arg NH2	2.90
14 Asp N	47 Val O	2.81

S-peptide	Water-Mediated Hydrogen Bonds[a] S-protein	distance (Å)
4 Ala O	118 Val O	2.90; 2.74
5 Ala O	117 Pro O	3.06; 2.73
9 Glu OE2	55 Gln NE2	3.00; 2.80

Change in Accessible Surface Area of Nonpolar Atoms[b] S-peptide		S-protein	
4 Ala	35.2 (CB)	33 Arg	17.1
5 Ala	34.2 (CB)	35 Leu	29.0 (CG, CD2)
8 Phe	114.5 (CB, CD1, CE1, CE2, CZ)	46 Phe	19.1 (CD1)
10 Arg	34.3 (CG, CD)	48 His	28.0
11 Gln	15.0	51 Leu	66.2 (CD1, CD2)
12 His	68.1 (CB, CE1)	54 Val	18.6 (CG1)
13 Met	67.1 (SD, CE)	116 Val	22.3 (CG2)
14 Asp	40.2 (CB)	118 Val	44.5 (CG1)
		120 Phe	36.5 (CB)

Area Changes: Sums over All Affected Atoms	S-peptide	S-protein
total ΔA (polar)[c]	316.2	235.6
total ΔA (nonpolar)[c]	468.3	376.5
grand total[c]	784.5	612.1

[a] The first distance is from the atom in column 1 to the water molecule. The second distance is from the water molecule to the atom in column 2. [b] Changes in the accessible surface area (ΔA) were calculated by taking a differences between accessible areas of S-peptide or S-protein alone and in the complex. Residues 16–23 are excluded from the calculation. Only the residues with a total area change of $\Delta A \geq 15$ Å^2 for the nonpolar atoms are tabulated, and the individual atoms with $\Delta A \geq 10$ Å^2 are listed in parentheses. [c] Totals and grand totals refer to a total change in the accessible area for all atoms, not just those listed above.

The backbone torsion angles, ϕ and ψ, are almost identical in the three structures. All the non-glycyl residues are within the allowed regions of the ϕ–ψ plot except for residue Gln60. The rms deviation of ω from 180° is 5.2°. Among the four prolines present, two (Pro42 and -117) are in the "trans" configuration while the other two (Pro93 and -114) are in the "cis" configuration. Both "cis" prolines are involved in sharp turns between β-regions, and they are well-defined in both $2F_o - F_c$ and omit maps. The prolines in RNase-A are in the same configurations. The distribution of χ_1 angles of the side chains is trimodal (g^-, t, and g^+) and is very similar to the rotamer library values reported by Ponder and Richards (1987).

The electron density around Gln60, as shown in Figure 2, is rather clear, and ϕ and ψ angles of −100° and −130° are observed in all three structures. Gln60 is at the end of the 50–60 mixed α–3_{10} helix. The OE1 atom of Gln60 makes a hydrogen bond to the backbone amide of 76 (OE1···N, 3.02

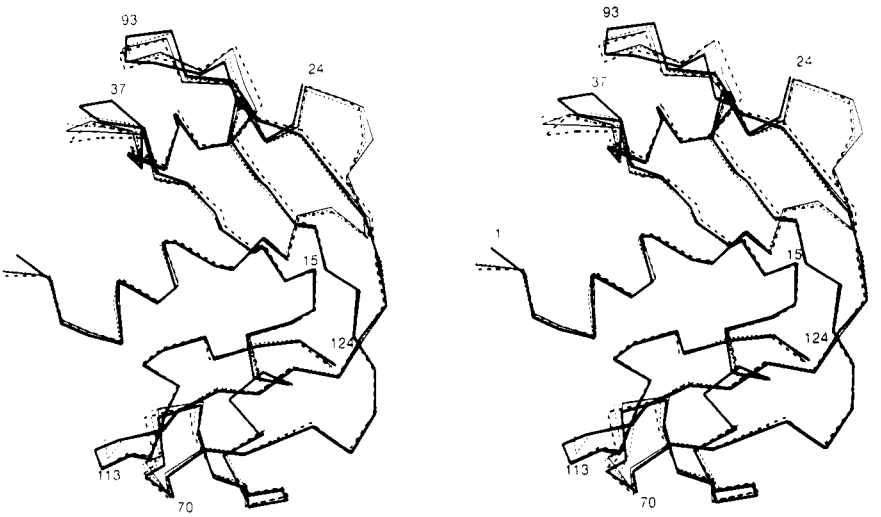

FIGURE 1: Cα trace of various RNase structures in stereo: RNase-S (heavy solid line) with residues 16–23 omitted, 7RSA (light solid line), 1RSM (dashed line), and 1SRN (light dashed line). The structures were superposed using INSIGHT. Cα, N, C, O, and Cβ atoms of residues 24–123 were used during the superpositioning procedure.

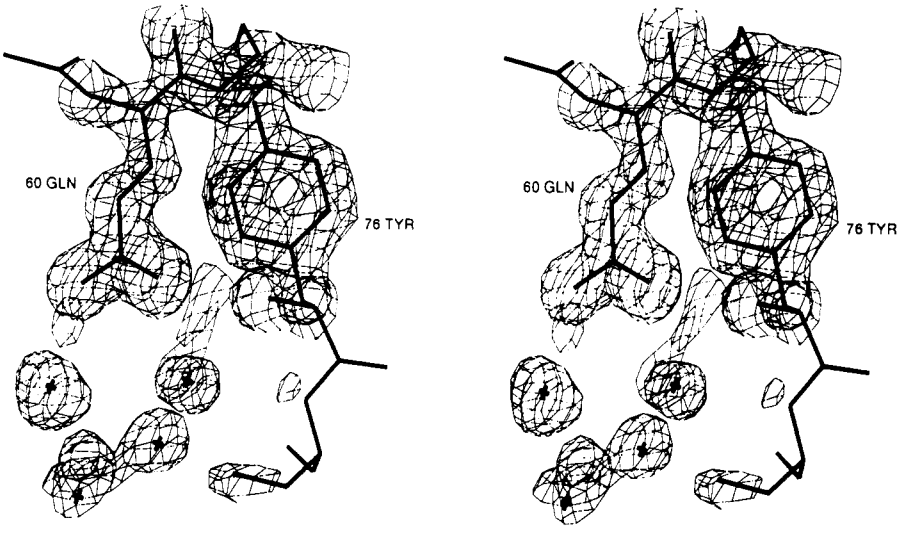

FIGURE 2: Electron density map around residue Gln60. This map was calculated with the coefficients $2F_o - Fc$, α_c from S20, pH 4.75, and is contoured at the 1.5σ level. Water positions are indicated by a +.

Å) and to a water (OE1···OW, 2.73 Å), which is hydrogen bonded to the amide of 77 (OW···N, 2.86 Å). Residues 76–78 bulge out from the β-strand. The NE2 of Gln60 makes a hydrogen bond to a water molecule (NE2···OW, 2.88 Å), which in turn hydrogen bonds to the carbonyl oxygen of Asp53 (OW···O, 2.98 Å). No other hydrogen bonds are detectable for the carbonyl oxygen of Asp53. The two waters are also hydrogen bonded to a third water. This pattern is seen in all three structures. Similar ϕ and ψ values are found for Gln60 in all RNase-A structures, and this is further discussed in the Comparison with RNase-A section.

(*b*) *Thermal Parameters.* The average thermal parameters for the backbone and side-chain atoms for all three structures are listed in Table I. The average temperature factors for the backbone atoms of S20, pH 4.75, are shown in Figure 7, below.

Throughout the refinement we have used three types of restraints on the isotropic thermal parameters. The three restraints used are (a) the conventional values of Hendrickson (1985), (b) the values reported by Yu et al. (1985) based on a simulation where side chain atom positions are allowed to vary more, and (c) no restraints at all.

The following observations are from the refinement where each residue is modeled in a single conformation. The average temperature factor plots (available as supplementary material), similar to Figure 7, show that the curves from (a) are much smoother than those from (c). The average temperature factors of the side-chain atoms are more sensitive to the types of restraints used than those of the main-chain atoms. Also, the regions with secondary structure show very little change in the temperature factors while the loop regions show larger variations. Although the *R*-values seem rather sensitive to the nature of the restraints used [differ by about 2.0% between (a) and (c)], the resulting electron density maps from all three are basically the same except that the map from (a) shows more connected density. The residue types that are most affected by the nature of the restraints are Ser, Lys, and Gly.

However, when some of the residues are modeled in two conformations, not only is the average temperature factor for the particular side chain reduced but also the average temperature factors for the main-chain atoms around the residues are lowered. Application of restraints on the temperature factors made less difference when multiple sites were included instead of single conformations.

(*c*) *Disordered Residues and Multiple Conformations.* There are several residues whose side chains are disordered. These are located mostly on the surface of the molecule. When

Table III: Side Chains in Two Conformations in RNase-S[a]

residue	conf	occupancy	⟨*B*-factor⟩[b] (Å²)	torsion angles (deg)			
				χ_1	χ_2	χ_3	χ_4
Gln28	a	0.60	62.4	−70	−174	142	
	b	0.40	37.5	−174	82	2	
Met29	a	0.50	15.9	−166	58	84	
	b	0.50	14.8	−80	−64	−79	
Lys31	a	0.60	57.0	−156	167	58	−176
	b	0.40	53.0	171	−144	166	−173
Ser32	a	0.60	53.6	−179			
	b	0.40	53.2	−67			
Leu35	a	0.40	18.4	−54	177		
	b	0.60	12.0	−78	83		
Val43	a	0.45	14.4	−64			
	b	0.55	15.8	−163			
Lys61	a	0.30	42.1	−43	−143	−31	104
	b	0.70	53.0	179	154	51	−171
Gln69	a	0.50	63.5	−101	−49	−88	
	b	0.50	60.8	−50	−61	−83	
Asp83	a	0.50	37.5	−69	117		
	b	0.50	14.3	117	89		
Arg85	a	0.35	34.4	−151	103	−170	174
	b	0.65	24.3	−170	92	−169	−176
Asn113	a	0.55	46.1	168	39		
	b	0.45	36.1	−88	98		

[a] These data are taken from the S20, pH 4.75, refinement. The residues in S15 are 29, 32, 35, 43, 77, 83, 85, and 98. Residue 77 is Ser and residue 98 is Lys. In RNase-A residues 11, 32, 34, 43, 50, 61, 67, 77, 83, 85, 91, 98, and 104 are modeled in two conformations (Svensson et al., 1986). [b] *B*-factors are averaged values for the side-chain atoms only.

the $2F_o - F_c$ maps were contoured at the 0.8σ level, the electron density around 11 residues showed clear branching and positive peaks in the difference map. This was true for both S20 structures. These were modeled in two discrete conformations. The results are summarized in Table III. The positive peaks in the difference map disappeared after modeling, and no new negative peaks appeared. As a further confirmation, the maps for some of these residues were generated after simulated annealing with those parts of the molecule omitted. In the case of S15 eight residues could be modeled in alternate conformations with confidence. It is interesting to note that the six protocols for S15 (see section g) also indicate disorder by giving different solutions for some of these residues. Many of these multiple sites are clustered in space; for example, Asp83, Arg85, and Val43 are within a 10-Å sphere. Many of the same residues were found in multiple conformations in all three structures.

In the final cycles of refinement after slow cooling protocols, 30 cycles of positional refinement were performed, followed by alternating steps of temperature factor refinement (15 steps) and occupancy factor refinement (15 steps). The starting parameters were set to 0.5 for the occupancy factor and 20.0 for the temperature factor for all atoms that are modeled in multiple conformations. At the end of 150 steps, the occupancy factors were adjusted so that the total for both conformations was 1.0, and an additional 120 steps of alternating positional refinement (30 steps) and temperature factor refinement (30 steps) were performed. The resulting average temperature factors for the side-chain as well as backbone atoms of these residues were lower than the values obtained describing them as single conformers.

(*d*) *Waters.* In addition to 1 sulfate ion at the active site, 84 water molecules, in the case of S20, pH 4.75, were located during the refinement. The *R*-value becomes 4–5% higher in each case if these are excluded in the structure factor calculation as seen in Table I. Twenty water molecules have the accessible surface of 0.0 as they appear in the crystal lattice; i.e., they are buried from bulk solvent. All except 7 waters make at least one hydrogen bond with protein atoms. Eighteen waters interact with neighboring symmetry-related molecules. The distribution of most of the waters is almost identical in the three structures.

In addition to the eight direct hydrogen bonds between the S-peptide and S-protein, there are three water molecules that bridge the two (see Table II). Also, at the amino end of the 3–13 helix, there are nine additional waters that are within a distance of 5 Å from both the S-peptide and S-protein. Many of these waters have temperature factors of less than 30 Å, and they appear to play a role in stabilizing the complex.

Kundrot and Richards (1987b) suggested that it is not appropriate to vary both temperature and occupancy factors for solvent atoms unless the resolution of the data is better than 1.0 Å, based on their model calculation. However, this conclusion has been disputed by Bhat (1989) and by Jensen (1990). In this study we examined this problem in the following calculation using the actual data from S20, pH 4.75. Initially both the occupancy and the temperature factors were set to fixed values; then 130 steps of refinement were carried out. In the first 15 steps only the atomic positions were refined. For the next 100 steps the atomic positions were held constant, and alternating cycles of temperature factor refinement (10 steps) for all atoms and occupancy factor refinement (10 steps) for water oxygens were performed. For the remaining 15 steps only the atomic positions were refined again. The procedure was carried out several times using starting values of 1.0, 0.75, 0.50, and 0.25 for the occupancy and 20.0 for the temperature factor of each water. Starting temperature factors of 50.0 and 70.0 with a starting occupancy of 1.0 were also tried. During each of these calculations, all protein atoms were fixed at an occupancy of 1.0. The final occupancies and temperature factors in each case depended on the starting values; therefore, convergence was not complete. For example, when starting with $B = 20.0$ and an occupancy of 0.5, the final occupancy on the average was 0.11 lower than when the starting occupancy was 1.0.

In each case the final coordinates and both $2F_o - F_c$ and difference maps were compared with those obtained using occupancies fixed to 1.0 and varying only the temperature factors for all atoms. In all cases the *R*-values as well as the resulting electron density maps were virtually identical with only minor exceptions with a few waters. Hence, for this data set at least, it does not appear to be possible to favor one procedure over the other.

(*e*) *Active Site.* The active site of RNase (Figure 3) is formed by the side chains of His12, Lys41, Val43, Asn44, Thr45, His119, Phe120, Asp121, and Ser123 (Richards & Wyckoff, 1971). In addition, there is 1 sulfate ion located in all three structures examined here. All the active site residues except His119 are well-defined in all three electron density maps. The side-chain atoms of Val43 are modeled in two conformations (see Table III). In the case of His119, although the electron density on the imidazole ring of His119 is not as well-defined as for other histidines in the structures, it appears that it is primarily in the one position as shown by the solid line. This is confirmed in the omit map as well as after simulated annealing. It should be noted that this is one of the four possible positions suggested (Richards & Wyckoff, 1971) and is different from the position in the presence of adenine-containing analogues (Wyckoff et al., 1977) which is shown by the dashed line. This if further discussed in the Comparison of RNase-A section.

Three of the oxygen atoms on the sulfate form four tight hydrogen bonds (less than 2.90 Å) to the protein atoms: NE2

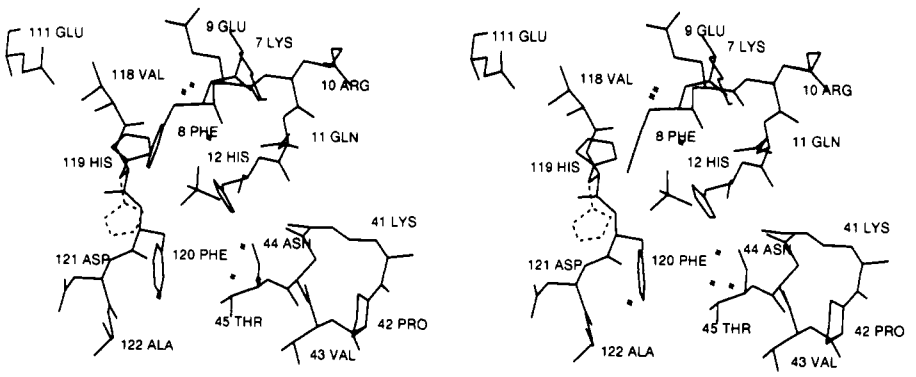

FIGURE 3: Stereoview of the active site of RNase-S. His119 is shown in two positions. The solid line shows the position found in all three structures reported here, while the dashed line shows the position observed in some other studies. These are referred to as up and down positions, respectively.

of His12, ND1 of His119, and the backbone amide of Phe120. The sulfate oxygens also form two hydrogen bonds to a water molecule, which, in turn, is hydrogen bonded to OE1 of Gln11. The conformations of all the residues in the active site are identical in all three structures except that the orientation of the imidazole ring of His119 seems to vary slightly from one structure to another.

(f) Intermolecular Packing. In the Y-form of the RNase-S there are extensive intermolecular interactions. Six molecules contact the central molecule at eight different patches, P, Q, R, S, T, U, V, and W. The accessible surface area lost due to crystal packing is 43% of the area for an isolated molecule, and almost 60% of this is from nonpolar atoms. Table IV lists intermolecular hydrogen bonds and the changes in the accessible surface areas associated with these patches. All of the changes in the accessible surface areas listed in Table IV refer to the difference in the areas between the isolated molecules and the molecules in the configurations related by the symmetry operations listed in the table.

The interactions in the P·Q pair are between two molecules related by a 2-fold rotation at $z = 0$. Figure 4a shows this interaction looking down the 2-fold axis. The two molecules form a dimer with the two active sites in close proximity (the two sulfate ions are approximately 20 Å from each other) and a hole along the 2-fold axis. The Arg85 protrudes into the active site of the companion molecule, making a salt bridge to Asp121.

The combination of the 2-fold at $z = 0$ along $y = x$, mentioned above, with another 2-fold translated along the b-axis ($y = x + 1$) produces a 2-fold screw axis at $z = 0$ that is parallel to the 2-fold rotation axes along $y = x + {}^1/_2$. This 2-fold screw produces two equivalent tight contacts. The patch R on the central molecule contacts the patch S on an adjacent molecule, and the patch S on the central molecule contacts the patch R of the molecule which is shifted by one unit cell from the first companion along the 2-fold screw axis. This interaction includes stacking of Tyr25 against Tyr92 of an adjacent molecule. Figure 4b shows the R·S interaction. The helix 24–34 stacks along this 2-fold screw axis at about an angle of 30°.

The remaining tight contacts are along the 2-fold screw at $z = {}^1/_6$ and $z = {}^1/_2$ that is parallel to the b-axis. As in the R·S pairs, this generates two molecules contacting the central molecule that are related by one unit cell translation. The 50–60 helix is at an angle of nearly 45° to this 2-fold axis, which is shown as a vertical line in Figure 4c. The helix 3–13 is almost perpendicular to the screw axis.

The interactions seen in the V·W pair are less extensive than the three mentioned above and involve a molecule that is related by 2-fold rotation at $z = {}^1/_6$ parallel to the b-axis.

The contacts along the 2-fold screw axes produce chains of contacting molecules running at 60° to each other. These combined with the 2-fold dimer relationships produce the three-dimensional network of contacts needed to sustain a crystal.

(g) Error Estimation. The overall mean errors in the atomic coordinates are estimated to be about 0.18 Å in all three

Table IV: Intermolecular Hydrogen Bonds in RNase-S[a]

		distance[b] (Å)
patch =P=	patch =Q=	
62 Asn O	88 Gly N	3.29
64 Ala O	85 Arg NE	3.04
64 Ala O	85 Arg NH1	2.69
64 Ala N	86 Glu O	3.00
66 Lys N	85 Arg NH1	3.25
121 Asp OD2	85 Arg NH1	2.72
121 Asp OD2	85 Arg NH2	3.21
123 Ser O	104 Lys NZ	3.11
124 Val OT2	104 Lys NZ	3.05
patch =R=	patch =S=	
38 Asp O	25 Tyr N	2.80
39 Arg NH2	24 Asn N	3.00
91 Lys NZ	14 Asp OD1	2.88
91 Lys NZ	15 Ser O	3.32
patch =T=	patch =U=	
1 Lys N	49 Glu OE2	3.01
33 Arg NE	59 Ser OG	2.92
33 Arg NH1	59 Ser O	2.93
37 Lys NZ	55 Gln OE1	3.06
patch =V=	patch =W=	
69 Gln OE1	112 Gly O	3.40

molecule A	molecule B	symmetry operation[a]
P 1	Q 2	$y, x, -z$
Q 1	P 2	$y, x, -z$
	ΔA = 427.8 (polar) + 602.1 (nonpolar)	
R 1	S 3	$y, 1 + x, -z$
S 1	R 4	$-1 + y, x, -z$
	ΔA = 256.0 (polar) + 358.9 (nonpolar)	
T 1	U 5	$-1 - x, y - x, {}^1/_3 - z$
U 1	T 6	$-1 - x, -1 + y - x, {}^1/_3 - z$
	ΔA = 506.7 (polar) + 546.7 (nonpolar)	
V 1	W 7	$-x, y - x, {}^1/_3 - z$
W 1	V 7	$-x, y - x, {}^1/_3 - z$
	ΔA = 104.8 (polar) + 72.0 (nonpolar)	

[a] Patches P, Q, R, S, T, U, V, and W represent different parts of the molecule. The numbers next to the patch designate different molecules, and these are generated by the symmetry operation listed. ΔA refers to the total area change in the accessible surface for both patches between the isolated molecules and the molecules as in the given configuration. Thus the area change associated with each patch will be half this amount. The components P·Q and V·W of patches are related by a 2-fold rotation while those of R·S and T·U are related by a 2-fold screw. [b] Hydrogen bond distances are from S20, pH 4.75.

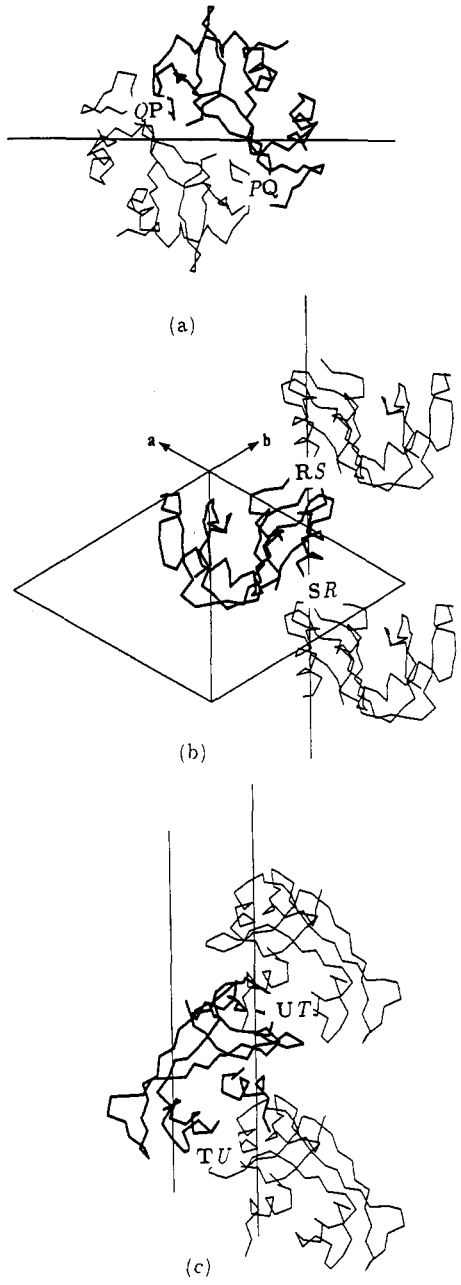

FIGURE 4: Cα drawing of neighboring molecules. The central molecule is shown by a heavy line with the patches labeled, while the symmetry-related molecules are shown by light lines. The positions of the relevant symmetry axes are also indicated. (a) P·Q patches: the molecules are related by a 2-fold axis at $z = 0$ and viewed looking down the 2-fold axis with the *ab* base plane horizontal and represented by a line. (b) R·S patches: the molecules are related by a 2-fold screw axis at $z = 0$. The 2-fold axis described in (a) is shown vertically in the *ab* plane. (c) T·U patches: the molecules are related by another 2-fold screw axis at $z = {}^1/_6$. The *ab* base plane is on the right of the 2-fold screw axis.

structures using the method of Luzzati (1952). This value is comparable to the values reported for *Escherichia coli* thioredoxin (1.68 Å; Katti et al., 1990) and α-chymotrypsin (1.67 Å; Blevins & Tulinski, 1985). However, this number is an average value, and it assumes that all the differences between the observed and calculated structure factors are due to a normally distributed positional error. Certainly, some atoms can be positioned better than this estimated value while the error of those with larger thermal parameters will have considerably larger values. Therefore, in order to obtain an independent estimate in the coordinate error, we have carried out a more extensive analysis using different runs of simulated annealing using X-PLOR. The S15 data set was used since it will provide an upper limit for the error. The results from six protocols are comparable in *R*-value and stereochemistry as well as in temperature factors. Also, the resulting electron density maps were comparable in quality.

The rms difference in position between the various protocols ranges from 0.050 to 0.088 Å for the backbone (C, N, Cα) atoms and from 0.42 to 0.67 Å for the side-chain atoms with average values of 0.069 and 0.49 Å, respectively. Ninety-four percent of the atoms have an rms deviation less than 0.1 Å. The rms deviations from the mean values are 0.048 Å for the backbone atoms and 0.34 Å for the side-chain atoms. The variations at individual atoms for some residues are shown in Table V. When the average rms difference for the backbone atoms is plotted against the residue number (available as supplementary material), it correlates highly with the average temperature factor. The core of the structure is quite rigidly maintained while the loops on the surface have variations from one protocol to another. The four ends of the molecule are certainly more mobile than other parts. There are several residues whose side-chain atomic positions differ from one protocol to another. These are mainly charged or polar residues (Lys, Gln, Glu, Asn, and Asp), and they are all located on the surface of the molecule. These are also the residues that are poorly defined in the electron density maps. Other flexible residues are Leu35, Val43, Ser77, and Ile81. Some of these are indeed the residues that could be modeled in two discrete conformations as shown in Table III.

(*2*) *Comparison with RNase-A.* Several RNase-A structures have been previously reported, and they are summarized in Table VI. These studies vary not only in crystallization conditions (i.e., solvent, ionic strength, and pH) and space group but also in the modes of data collection and refinement.

(*a*) *Overall Structure* (*Cα and φ/ψ*). The structures are compared using difference distance plots (Kundrot & Richards, 1987a) where the changes in the distance between corresponding pairs of Cα atoms in two different molecules are examined. In the plot the regions that are featureless indicate that the two structures are identical within the range of the distance cutoffs used, while the regions with changes are shown as contours, thick lines representing distance increases and thin lines representing distance decreases. It is contoured from 0.5 to 2.0 Å at intervals of 0.5 Å. We have examined all RNase-A structures with respect to RNase-S and also compared different RNase-A structures with each other. Some are shown in Figure 5. The upper and lower triangles show two different plots. Figure 1 shows the Cα traces after superposition (see Materials and Methods for details).

As expected, the overall structures of RNase-A and -S are very similar in all cases except near the cleavage site. Residues 16–23 differ appreciably between RNase-S, where they are disordered, and RNase-A, and they are omitted from Figure 5. However, it should be noted that it is impossible to have these residues in the same orientation as in RNase-A due to crystal packing in the RNase-S Y-form crystals used in these studies. Differences around residues 113 and 114 in the case of 1SRN should be ignored for the same reason.

All the RNase-A structures in the $P2_1$ space group show very similar patterns when compared to RNase-S. The RNase-A structures, determined in different laboratories but in the same space group, show practically no difference from one another at the 0.5-Å contour level used in Figure 5. The magnitude of the differences between RNase-A structures in different space groups is somewhat smaller than those seen

Table V: Position Variability in Six X-PLOR Runs on the S15 Complex[a]

	α	β	γ	δ	ε	ζ	η		α	β	γ	δ	ε	ζ	η
1 Lys	2	1	11	12	12	9		69 Gln*	2	3	16	13	28, 37		
7 Lys	1	1	2	3	13	22		77 Ser*	1	2	16				
28 Gln*	2	5	20	36	96, 29			81 Ile	1	2	2, 2	14			
29 Met*	1	1	11	1	4			85 Arg*	3	8	34	11	7	3	2, 5
31 Lys*	2	5	17	15	48	29		91 Lys	1	2	7	13	9	30	
35 Leu*	1	1	2	14, 11				98 Lys*	1	2	5	11	5	35	
37 Lys	1	2	7	13	14	36		103 Asn	1	2	6	23, 5			
39 Arg	2	5	22	27	14	11	43, 15	111 Glu	2	3	4	10	16, 13		
43 Val*	3	10	47, 57					121 Asp	2	2	4	6, 5			
61 Lys*	1	2	4	7	34	57		123 Ser	4	4	10				
66 Lys	4	12	31	8	36	80		124 Val	3	5	14, 16				

[a] Distances are in units of 0.01 Å. All residues in which any atom has an rms variation from the mean >0.1 Å are listed. Residues marked with an asterisk were modeled using two conformations in the refinement procedure. Residues 16–23 were omitted.

Table VI: Results of Refinement and Crystallization Conditions

code[a]	res (Å)	R-factor (%)	rms[b] bond (Å)	no. of waters, others	data collection conditions	space group; cell parameters
				Ribonuclease S		
S20 (2RNS)	1.60	17.4	0.013	84 1 SO_4	75% $(NH_4)_2SO_4$, 0.1 M $NaCH_3COO$ (pH 4.75, 5.5)	$P3_121$; 44.50, 44.50, 97.62 Å
S15 (1RNV)	1.60	18.6	0.013	70, 1 SO_4	same as above	same as above
				Ribonuclease A		
7RSA	1.26	15.0	0.024	188, 1 *t*-BuOH	43% *t*-BuOH (pH 5.3)[c]	$P2_1$; 30.18, 38.40, 53.32 Å; 105.9°
5RSA	2.0	15.9 (X),[d] 18.3 (N)[d]	0.23	128, 1 PO_4	55% *t*-BuOH (pH 5.3), 10 mM phosphate	same as above
6RSA	2.0	18.8 (X),[d] 19.9 (N)[d]	0.23	112 1 UV[d]	25% MeOD, 12.3 mg/mL uridine vanadate, imidazole (pH 6.8)	same as above
1RN3	1.45	24.0	0.01	78, 1 SO_4	60% aqueous EtOH (pH 5.2–5.7)	$p2_1$; 30.4, 38.4, 53.2 Å; 106°
WSO4	1.53	17.0			70% aqueous EtOH (pH 6.8)	$P2_1$; 30.15, 38.18, 53.14 Å; 106.4°
PAUL	2.13	18.0	0.014	80, 2 SO_4	75% $(NH_4)_2SO_4$, 0.1 M $NaCH_3COO$ (pH 4.75)	$P3_221$; 64.9, 64.9, 65.22 Å
				Modified Ribonuclease A		
1RSM	2.0	18.4	0.024	75, 1 PNP[e]	30% aqueous EtOH,[c] 50 mM imidazole (pH 8.0)	$P2_12_12_1$; 37.05, 41.26, 75.64 Å
8RSA	1.77	16.2	0.016	246, 2 dT[e]	80% $(NH_4)_2SO_4$, $NaCH_3COO$ (pH 5.1)	$P2_12_12_1$; 53.14, 64.10, 73.15 Å
9RSA	1.77	19.6	0.016	181, 2 dU[e]	same as above	same as above; 52.75, 64.61, 73.64 Å
1SRN	1.8	20.4	0.024	115, 1 SO_4	80% $(NH_4)_2SO_4$, 0.1 M $NaCH_3COO$ (pH 5.2)	$P3_221$; 67.68, 67.68, 65.03 Å

[a] File names are from the Protein Data Bank (Berstein et al., 1977) except WSO4 and PAUL: 7RSA, Wlodawer et al. (1988); 5RSA, Wlodawer et al. (1983); 6RSA, Borah et al. (1985); 1RN3, Borkakoti et al. (1982); WSO4, Campbell and Petsko (1987); PAUL, Harkins, personal communication; 1RSM, Weber et al. (1985); 8RSA, Nachman et al. (1990); 9RSA, Nachman et al. (1990); 1SRN, Martin et al. (1987). [b] These root-mean-square (rms) values are the differences between observed and ideal values. The set of ideal values differs among the authors; thereby, the rms values may not be comparable. [c] Crystallization conditions. The data collection conditions were not stated. [d] (X) is the *R*-factor using X-ray data while (N) is the *R*-factor from the neutron data. [e] UV = uridine vanadate; PNP = dinitrophenylene; dT = *N*-acetylthymidine; dU = *N*-acetyldeoxyuridine.

between RNase-S and RNase-A, despite the fact that some of the RNase-A structures are chemically modified. There is a slight systematic displacement of segments of the β-sheet structure (see Figure 1) which may be meaningful, but larger displacements seen in the loop regions are discussed below.

Regions 36–39, 66–69, 88–96, and 110–114 are different in all ribonuclease structures. The differences are above the estimated errors in the coordinates. This is true among crystallogaphically independent RNase-A structures. Since some of these RNase-A structures involve either chemical modifications or fragmentation, the differences observed may result from such changes.

However, it is interesting to note that residues 36–39 of RNase-S are distinctly different from the cluster of RNase-A structures as seen in Figures 1 and 5. This region is distant from the cleavage site, and helix 24–34 is almost identical in all the structures. The difference distances between Cα positions at residues 37 and 38 are well over 2.0 Å.

The Ramachandran plots for the RNase-A structures are very similar to that of RNase-S. Gln60 is certainly an outlier with similar ϕ and ψ values as in RNase-S. The energy associated with such ϕ/ψ angles is about 3 kcal (using CHARMM; Brooks et al., 1983). H-bonds to Q60 may be enough to overcome this ϕ/ψ energy penalty. The two waters mentioned for RNase-S that are associated with the side chain of Gln60 appear to be structurally important since they are also seen in all of the RNase-A structures except 1RN3. It should be noted that Gln60 is an invariant residue in a series of ribonucleases (Beintema et al., 1988).

The backbone dihedral angles of residues 37 and 38 are quite different: the ϕ of Asp38, in particular, differs by more than 40° (−132° in RNase-S and around −90° in RNase-A). Other loops have differences between RNase-S and the different RNase-A structures spread out with somewhat smaller Cα–Cα difference distances. The standard deviations for both ϕ and ψ are plotted as a function of residue number in Figure 6.

(*b*) *Stereochemistry of the Side Chains and Some of the Water Structures.* The overall distribution of the χ_1 angles of side chains is trimodal and close to the distribution reported by Ponder and Richards (1987). The RNase-A residues that are internal have χ_1 values almost identical to those of RNase-S. The conformations of some of the residues on the surface are also the same as in RNase-S, and these are mainly the ones that are involved in the intramolecular H-bonding. Many of the residues on the surface are quite flexible, and conformations vary from one structure to another. Five of the residues in Table III are also found in multiple conformations in RNase-A (Svensson et al., 1986).

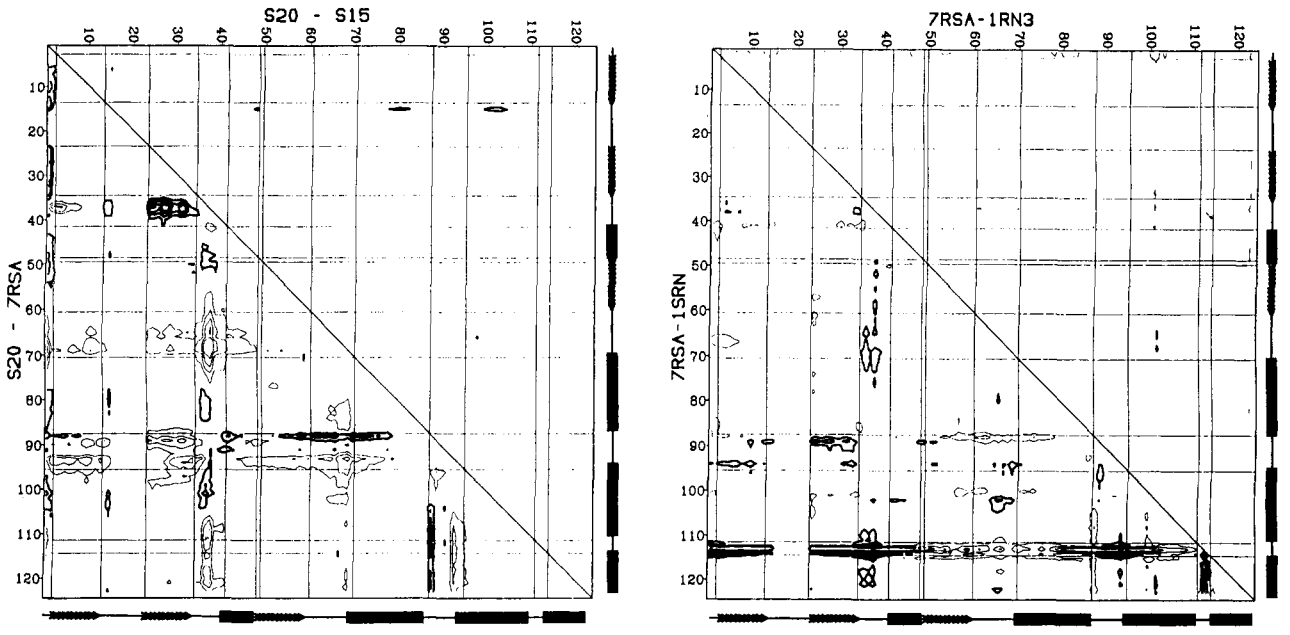

FIGURE 5: Difference distance plots between Cα atoms. Thick lines represent distance increases while thin lines represent distance decreases. Contouring levels of 0.50 Å were used starting from 0.50 Å. The upper and lower triangles each contain a different plot: (a) upper, S20 vs S15; lower, S20 vs 7RSA; (b) upper, 7RSA vs 1RN3; lower, 7 RSA vs 1SRN. The secondary structure is shown on the right and bottom (for helices and for strands).

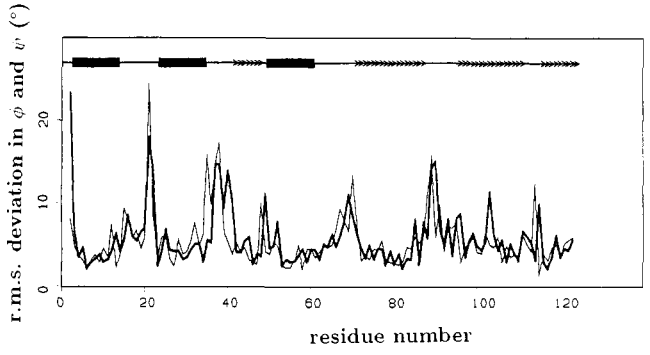

FIGURE 6: Standard deviations in the backbone dihedral angles shown as a function of residue number: ϕ (heavy line) and ψ (light line). All the structures in Table VI are included in the calculation. Residues 16–23 of RNase-S are omitted in the calculation.

The residues in the active site are similar in their orientations except for Val43 and His119. The latter is in two distinctly different conformations ("up" and "down"). Since in the early studies His119 was so poorly defined, Richards and Wyckoff (1973) suggested the possibility of four different conformations for this residue. Borkakoti et al. (1982) reported His119 in two conformations with occupancies of 0.8 and 0.2 in 1RN3. All others including this study find it in only one conformation. The χ_1 values are around –60° (up position) in RNase-S, 1SRN, and PAUL and 180° (down position) in all other structures. The three structures with χ_1 values of –60° and 1RN3 were crystallized from high salt and include a sulfate in the active site, to which His119 is hydrogen bonded (see Figure 3). However, Palmer et al. (1984) reported His119 in exclusively the up position in RNase-A crystallized from aqueous alcohol when cytidine N^3-oxide 2′-phosphate (O(3)-2′CMP) is bound at the active site. Also, it does not appear that the conformation of His119 is due to the presence or absence of sulfate, since Campbell and Petsko (1987) and Wlodawer et al. (1988) found the histidine in the same conformation in either the absence or the presence of sulfate. In the absence of sulfate a water molecule occupies the position which is occupied by one of the sulfate oxygens when sulfate is present, as in 7RSA and 1RSM. The water structures are more difficult to compare, since the data are from crystals in different solvent systems and at different resolutions. However, some of the waters that are bound tightly to the protein are found in all strucures. For example, the water that is hydrogen bonded to one of the carboxyl oxygens of Asp53 and Glu49 and the amide of Ser50 is found in all structures except in the second molecules of 8RSA and 9RSA. Another example is the water hydrogen bonded to the carbonyl oxygens of Asp83 and Lys98 and the hydroxyl of Thr100. This is seen in all the structures except 1RN3. In some cases this water is further hydrogen bonded either to the carboxyl of Asp83 or to an additional water.

(*c*) *Thermal Parameters.* Figure 7 shows the average temperature factor for the backbone atoms. Only the backbone atoms were used in this comparison since they are less sensitive toward the types of restraints used for the refinement. Again, plots for structures in the same space group show basically the same pattern despite the fact that data were collected by different means and they were refined using different algorithms. It is clear that parts of the molecule that involve secondary structure have lower temperature factors and thus reflect the rigidity of the core. The loop regions, on the other hand, show much higher values than the core, and the magnitudes vary between the structures. This agrees with the results from the difference distance calculation. The average temperature factor for the backbone atoms was appreciably higher in RNase-S compared to 7RSA and 1RN3. This is consistent with increased susceptibility of RNase-S toward proteolytic digestion. However, it should be noted that the two RNase-A structures are at higher resolution and they were crystallized from different solvents.

(*d*) *Accessibility and Intermolecular Interactions.* Solvent-accessible surface areas were calculated both for an isolated molecule and for a molecule as found in the crystal lattice. The difference between the two areas, i.e., the surface buried due to crystal packing, reflects the degree of intermolecular

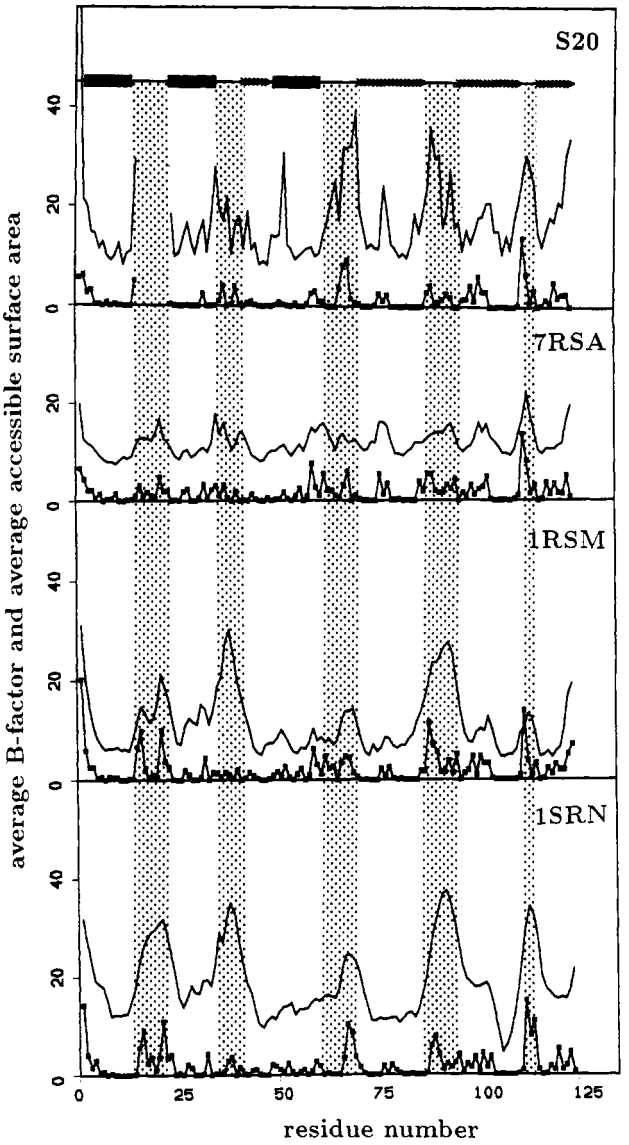

FIGURE 7: Average temperature factors and average accessible surface areas in the crystal lattice for the main-chain atoms as a function of residue number. The top line in each panel shows the temperature factors; the lower line, the accessibilities. The same ordinate in Å^2 applies to both lines. The plots for 1RN3 and WSO4 are very similar to that of 7RSA. Only the protein atoms are included in the calculations for accessible surface area. A probe size of 1.4 Å was used.

interaction. Water molecules were excluded in the calculation, since the number of water molecules varies from one data set to another and depends on the solvent used and the resolution of the data. The calculations show that the solvent-accessible areas of the isolated molecules are comparable, but the accessibility in the crystal lattice differs appreciably from one structure to another. The surface area buried is the largest for RNase-S (2750 Å^2; 43.0%) despite the fact that the other crystal forms have a larger number of neighboring molecules. Residues 16–23 of RNase-S are excluded in this calculation. The corresponding values for 7RSA, 1RSM, and 1SRN are 2005 (28.4%), 2140 (30.8%), and 1900 (28.3%) Å^2, respectively. In the case of RNase-S and 7RSA, these values are similar to the values reported by Crosio et al. (1990). The average accessible surface areas, as found in the crystal lattice, for the backbone atoms are depicted in Figure 7. The intermolecular interactions can be further examined by looking at the interatomic distances for the four loop regions in more detail, and this is available as supplementary material. Table VII lists the total change in the accessible areas for the four regions between the isolated molecule and the molecule in the crystal lattice. It is interesting to note that S20 and 7RSA have a similar number of interactions. These interactions are highly correlated with the general patterns observed for the thermal parameters and accessibility (Figure 7).

Table VII: Change in Accessible Surface Area for the Four Loop Regions[a]

residues	S20	7RSA	1RSM	1SRN
33–42	314.7	278.5	198.8	120.9
64–71	252.4	353.8	317.4	170.7
85–95	505.3	343.7	346.3	250.5
111–116	59.8	152.3	111.7	4.5

[a] ΔA refers to the total change in the accessible surface areas for the listed residues between the isolated molecule and the molecule in the crystal lattice.

It is interesting to note from Table VII that it can be seen that S20 and 7RSA have a similar number of interactions in the 36–39 region, yet they show large differences in Cα–Cα distances and dihedral angles in these residues. Also, 1SRN and 7RSA have the same structure in this region although the crystal packing interactions are quite different. This suggests that the differences between 7RSA and S20 are not solely determined by crystal contacts. Allende and Richards (1962) found that at room temperature RNase-A is indefinitely stable toward tryptic digestion while RNase-S is rapidly inactivated. RNase-A is cleaved by trypsin at elevated temperatures (60 °C) with initial cuts in the 31–38 loop region (Oi et al., 1963; Oi & Scheraga, 1964). It is tempting to speculate that these structural differences may be part of the reasons for the different behavior toward trypsin cleavage in RNase-A and RNase-S.

(*e*) *Refinement Using RNase-A as the Starting Model.* The structural differences in RNase-A and RNase-S were suggested earlier as being due to a possible error in the chain trace in either or both molecules (Wlodawer et al., 1982). Indeed, some of these regions, residues 66–69 of RNase-S in particular, are not clearly defined in the electron density maps. In order to remove any doubt that these differences are real, we have carried out refinements using RNase-S data starting with various RNase-A structures. Three models were used as described in Materials and Methods section c.

In all cases the final models were very similar to that obtained by starting from the earlier RNase-S model and were well within the estimated errors in the coordinates. Simulated annealing overcame errors in the chain trace, shifting the backbone atoms by 2.0 Å or more in the regions around residues 37–38 and 88–89. These results provide confidence in the structure of the region around 66–69 and the differences in the 36–40 region.

ACKNOWLEDGMENT

We are grateful to G. A. Petsko and P. Harkins for supplying coordinates and to A. Brünger, T. Simonson, and J. Wang for helpful discussions.

SUPPLEMENTARY MATERIAL AVAILABLE

Ramachandron plot, boundaries of secondary structures, average thermal parameters, six protocols and average rms deviations from the mean in the six runs, and detailed interatomic interactions for the residues in the four loop regions (6 pages). Ordering information is given on any current masthead page.

REFERENCES

Allende, J. E., & Richards, F. M. (1962) *Biochemistry 1*, 295.

Beintema, J. J., Schüller, C., Irie, M., & Carsana, A. (1988) *Prog. Biophys. Mol. Biol.* 51, 165.
Berstein, F. C., Koetzle, T. F., Williams, G. J. B., Meyer, E. F., Jr., Brice, M. D., Rodgers, J. R., Kennard, O., Shimanouchi, T., & Tasumi, M. (1977) *J. Mol. Biol. 112*, 535.
Bhat, T. N. (1989) *Acta Crystallogr. A45*, 145.
Blackburn, P., & Moore, S. (1982) in *The Enzymes* (Boyer, P. D., Ed.) 3rd ed., p 317, Academic Press, New York.
Blevins, R. A., & Tulinski, A. (1985) *J. Biol. Chem. 260*, 4264.
Borah, B., Chen, C., Egan, W., Miller, M., Wlodawer, A., & Cohen, J. S. (1985) *Biochemistry 24*, 2058.
Borkakoti, N., Moss, D. S., & Palmer, R. A. (1982) *Acta Crystallogr. B38*, 2210.
Brünger, A. T. (1990) *X-PLOR, Version 2.1*, Yale University, New Haven, CT.
Brünger, A. T., Kuriyan, J., & Karplus, M. (1987) *Science 235*, 458.
Brünger, A. T., Karplus, M., & Petsko, G. A. (1989) *Acta Crystallogr. A45*, 50.
Brünger, A. T., Krukowski, A., & Erickson, J. (1990) *Acta Crystallogr. A46*, 585.
Campbell, R. L., & Petsko, G. A. (1987) *Biochemistry 26*, 8579.
Connelly, P. R., Varadarajan, R., Sturtevant, J. M., & Richards, F. M. (1990) *Biochemistry 29*, 6108.
Crosio, M.-P., Rodier, F., & Jullien, M. (1990) *FEBS Lett. 271*, 152.
Doscher, M. S., & Hirs, C. H. W. (1967) *Biochemistry 6*, 305.
Finzel, B. C. (1987) *J. Appl. Crystallogr. 20*, 53.
Finzel, B. C., Kimatian, S., Ohlendorf, D. H., Wendoloski, J. J., Levitt, M., & Salemme, F. R. (1990) in *Crystallographic and Modeling Methods in Molecular Design* (Ealick, S., & Bugg, C. E., Eds.) p 175, Springer-Verlag, New York.
Hendrickson, W. A. (1985) *Methods Enzymol. 115*, 252.
Howard, A. J., Nieber, C., & Xuong, H. N. (1985) *Methods Enzymol. 114*, 452.
Jensen, L. H. (1990) *Acta Crystallogr. B46*, 650.
Jones, T. A. (1982) FRODO, in *Computational Crystallography* (Sayre, D., Ed.) p 303, Clarendon Press, Oxford.
Kartha, G., Bello, J., & Harker, D. (1967) *Nature 213*, 862.
Katti, S. K., LeMaster, D., & Eklund, H. (1990) *J. Mol. Biol. 212*, 167.
Kundrot, C. E., & Richards, F. M. (1987a) *J. Mol. Biol. 193*, 157.
Kundrot, C. E., & Richards, F. M. (1987b) *Acta Crystallogr. B43*, 544.
Lee, B., & Richards, F. M. (1971) *J. Mol. Biol. 55*, 379.
Luzzati, V. (1952) *Acta Crystallogr. 5*, 802.
Martin, P. D., Doscher, M. S., & Edwards, B. F. P. (1987) *J. Biol. Chem. 262*, 15930.
Nachman, J., Miller, M., Gilliland, G. L., Carty, R., Pincus, M., & Wlodawer, A. (1990) *Biochemistry 29*, 928.
Oi, T., & Scheraga, H. A. (1964) *Biochemistry 3*, 641.
Oi, T., Rupley, J. A., & Scheraga, H. A. (1963) *Biochemistry 2*, 432.
Palmer, R. A., Moss, D. S., Haneef, I., & Borkakoti, N. (1984) *Biochim. Biophys. Acta 785*, 81.
Ponder, J. W., & Richards, F. M. (1987) *J. Mol. Biol. 193*, 775.
Powers, T. B. (1976) Ph.D. Thesis, Yale University, New Haven, CT.
Ramachandran, G. N., & Sasisekharan, V. (1968) in *Advances in Protein Chemistry* (Anfinsen, C. B., Jr., Anson, M. L., Edsall, J. T., & Richards, F. M., Eds.) Vol. 23, p 283, Academic Press, New York.
Richards, F. M. (1985) *Methods Enzymol. 115*, 440.
Richards, F. M., & Vithayathil, P. J. (1959) *J. Biol. Chem. 234*, 1459.
Richards, F. M., & Wyckoff, H. W. (1971) in *The Enzymes* (Boyer, P., Ed.) Vol. 4, p 647, Academic Press, New York.
Richards, F. M., & Wyckoff, H. W. (1973) in *Ribonuclease-A. Atlas of Molecular Structures in Biology* (Phillips, D. C., & Richards, F. M., Eds.) Clarendon Press, Oxford.
Richards, F. M., & Kundrot, C. E. (1988) *Proteins: Struct., Funct., Genet. 3*, 71.
Rico, M., Bruix, M., Santoro, J., Gonzalez, C., Neira, J. L., Nieto, J. L., & Herranz, J. (1989) *Eur. J. Biochem. 183*, 623.
Sherwood, L. M., & Potts, J. T., Jr. (1965) *J. Biol. Chem. 240*, 3799.
Steigemann, W. (1982) Ph.D. Thesis, Technical University, Munich.
Svensson, L. A., Sjolin, L., Gilliland, G. L., Finzel, B. C., & Wlodawer, A. (1986) *Proteins: Struct., Funct., Genet. 1*, 370.
Takahashi, T., Irie, M., & Ukita, T. (1969) *J. Biochem. (Tokyo) 65*, 55.
Taylor, H. C., Richardson, D. C., Richardson, J. S., Wlodawer, A., Komoriya, A., & Chaiken, I. M. (1981) *J. Mol. Biol. 149*, 313.
Weber, P. C., Sheriff, S., Ohlendorf, D. H., Finzel, B. C., & Salemme, F. R. (1985) *Proc. Natl. Acad. Sci. U.S.A. 82*, 8473.
Wilmot, C. M., & Thornton, J. M. (1988) *J. Mol. Biol. 203*, 221.
Wlodawer, A., & Sjölin, L. (1983) *Biochemistry 22*, 2720.
Wlodawer, A., Bott, R., & Sjölin, L. (1982) *J. Biol. Chem. 257*, 1325.
Wlodawer, A., Svensson, L. A., Sjölin, L., & Gilliland, G. L. (1988) *Biochemistry 27*, 2705.
Wyckoff, H. W., Hardman, K. D., Allewell, N. M., Inagami, T., Tsernoglou, D., Johnson, L. N., & Richards, F. M. (1967a) *J. Biol. Chem. 242*, 3749.
Wyckoff, H. W., Hardman, K. D., Allewell, N. M., Inagami, T., Johnson, L. N., & Richards, F. M. (1967b) *J. Biol. Chem. 242*, 3984.
Wyckoff, H. W., Tsernoglou, D., Hanson, A. W., Knox, J. R., Lee, B., & Richards, F. M. (1970) *J. Biol. Chem. 245*, 305.
Wyckoff, H. W., Carlson, W., & Wodak, S. (1977) in *Nucleic Acid–Protein Recognition* (Vogel, H. J., Ed.) p 569, Academic Press, New York.
Yu, H.-A., Karplus, M., & Hendrickson, W. A. (1985) *Acta Crystallogr. B41*, 191.

Registry No. RNase S, 9001-99-4.